Molybdenum oxide nanowires: synthesis & properties

Molybdenum oxide nanowires have been found to show promise in a diverse range of applications, ranging from electronics to energy storage and micromechanics. This review focuses on recent research on molybdenum oxide nanowires: from synthesis and device assembly to fundamental properties. The synthesis of molybdenum oxide nanowires will be reviewed, followed by a discussion of recent progress on molybdenum oxide nanowire based devices and an examination of their properties. Finally, we conclude by considering future developments.

Liqiang Mai[a,b,*], Fan Yang[a], Yunlong Zhao[a], Xu Xu[a], Lin Xu[a,b], Bin Hu[a], Yanzhu Luo[a], and Hangyu Liu[a]

[a]*State Key Laboratory of Advanced Technology for Materials Synthesis and Processing, WUT-Harvard Joint Nano Key Lab, Wuhan University of Technology, Wuhan 430070, China*

[b]*Department of Chemistry and Chemical Biology, Harvard University, Cambridge, Massachusetts 02138, USA*

**E-mail: mlq@cmliris.harvard.edu*

The field of transition metal oxides represents an exciting and rapidly expanding research area that spans the border between the physical and engineering sciences[1-4]. Molybdenum oxides (MoO_x) are one of the most attractive metal oxides due to their special structural characteristics. MoO_x comprises two simple binary oxides, namely, MoO_3 and MoO_2. MoO_3 has several polymorphs, such as the thermodynamically stable α-MoO_3 (space group *Pnma*), metastable β-MoO_3 ($P2_1/c$), ε-MoO_3 ($P2_1/m$), and hexagonal metastable h-MoO_3 ($P6_3/m$)[5]. MoO_2, with its distorted rutile structure, is an unusual but interesting transition metal oxide because of its low metallic electrical resistivity (8.8×10^{-5} Ω·cm at 300 K in bulk samples), high melting point, and high chemical stability[6]. MoO_2 has been used as a catalyst for alkane isomerization[7-11], oxidation reactions[12], and as a gas sensor[13]. It is also a promising anode material for Li-ion batteries[14-18].

As nanotechnology has developed, nanostuctrues have received significant attention. Interesting physical phenomena appear as the scale of the building blocks approaches the nanoscale, such as the size effect, quantum conductance, and coulomb blockades. Nanowires are one of these building blocks that possess several distinct, practical properties, such as well-controlled dimensional composition, electronic radial transport, and crystallinity; this helps organize the nanoscale building blocks into assemblies and, ultimately, useful systems. Although research on molybdenum oxide (MoO_x) nanowires started relatively late, MoO_x nanowires are now showing potential for both fundamental research and applications in industry. MoO_x nanowires represent attractive building blocks for active nanodevices. By controlling the growth and organization, they can be used to produce a number of novel, highly-efficient, robust, integrated nanoscale devices, including field emission devices (FED) and photodetectors.

Nanowires and nanorods are typically cylindrical, hexagonal, square, or triangular in cross-section. Nanobelts are typically rectangular in cross-section, with highly anisotropic dimensions. In this article, nanobelts and nanorods are regarded as special kinds of nanowire.

ISSN:1369 7021 © Elsevier Ltd 2011

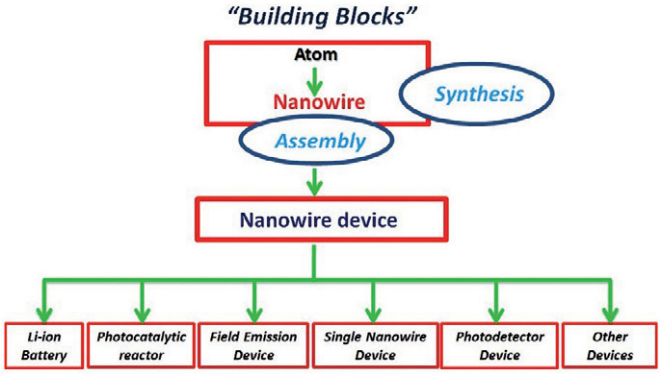

Fig. 1 "Bottom-up" fabrication procedure for MoOx nanowire devices.

Nowadays, the *bottom-up* technique is usually used for the assembly of MoO_x nanowires and devices. A bottom-up design necessitates building with precisely controlled nanomaterial parameters (including chemical composition and structure), which determine the final performance of the device[19,20]. Fig. 1 shows the bottom-up procedure for MoO_x nanowire device fabrication. To date, there has been no review that systematically summarizes the recent advances in MoO_x nanowires from synthesis to devices and their properties. In this article, we focus on recent advances on MoO_x nanowires based on our group's work.

Synthesis

Before 2000, nanomaterials based on molybdenum compounds, such as MoS_2[21,22], $MoSi_2$[23], $MoSe_2$[24], etc., had been investigated extensively. It is only during the last few years that MoO_x nanowires have attracted any attention in the literature. In 2000, Zach *et al.*[25] used the electrode position method to prepare MoO_x nanowires ranging from 20 nm to 1.3 μm in diameter for the first time. In the same year, carbon nanotubes were used as a template to synthesize α-MoO_3 nanowires with a diameter of 5 – 15 nm[26]. After that, various strategies were developed to design and rationally synthesize MoO_x nanowires with predictable control over the key structural, chemical, and physical properties. In 2001, Nesper *et al.*[27] synthesized molybdenum oxide nanowires with a high aspect ratio using a template-directed hydrothermal process. In 2003, Wang *et al.*[28] prepared nanowires of single-crystal α-MoO_3 without using a catalyst or template. In 2007, Mai *et al.*[29,30] synthesized α-MoO_3 nanowires, and for the first time lithiated α-MoO_3 nanowires to improve the electrochemical properties. A secondary reaction with a LiCl solution allowed the nanowires to retain their crystal structure and surface morphology, simultaneously. The crystallographic information and morphology can be seen in Fig. 2. In 2011, Cai *et al.*[31] synthesized flower-like α-MoO_3 nanowire arrays on diverse substrates using an atmospheric, catalyst-free, rapid flame synthesis technique. The growth rate, morphology, and surface coverage density of the α-MoO_3 nanowires were all controlled.

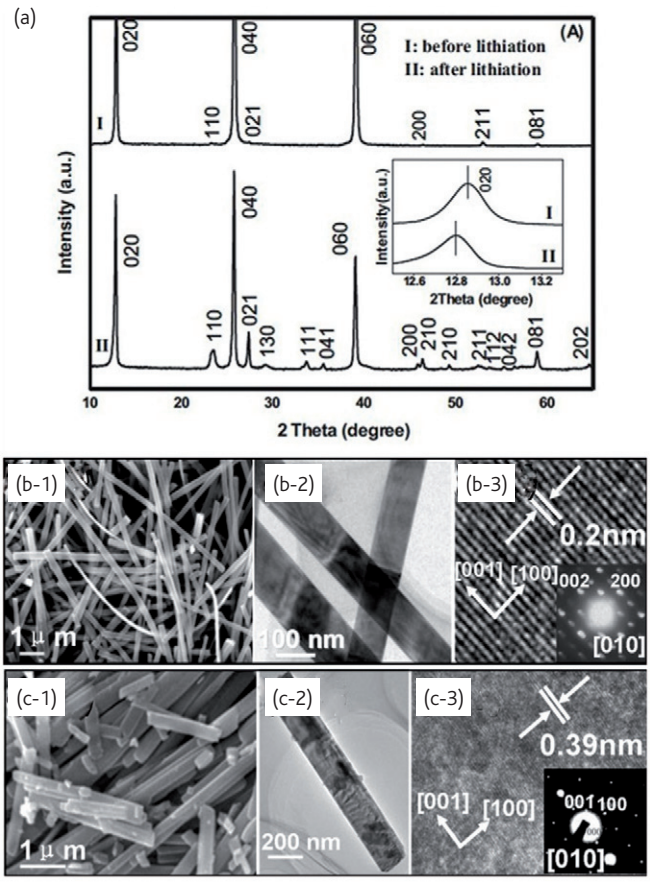

Fig. 2 (a) X-ray diffraction (XRD) patterns of an MoO_3 nanowire before and after lithiation. The inset is the corresponding (020) diffraction peak. (b),(c) SEM, TEM, and HRTEM characterization of the nanowire before and after lithiation, respectively. The insets in the HRTEM images are the corresponding selected area electron diffraction (SAED) patterns. Reprinted from[29]. © Wiley-VCH Verlag GmbH & Co. KGaA. Reproduced with permission.

MoO_2 is another important molybdenum oxide. The electronic configuration of Mo^{4+} is $4d^2$, and MoO_2 possesses a monoclinic structure[32]. MoO_2 is used extensively, in Li-ion batteries, field emission devices, catalysts, sensors, photochromic devices, and electrochromic devices, etc. In 2000, Satishkumar *et al.*[26] prepared MoO_2 nanowires using carbon nanotube templates. In this experiment, MoO_3 was first produced, and then heated in H_2 at 500 °C for 48 hours to prepare MoO_2 nanowires. Zhou *et al.*[33] produced nanowire arrays of MoO_x on silicon substrates based on a process of thermal evaporation followed by further oxidation (for the oxide ensembles). MoO_2 nanowire arrays were first grown on silicon substrates by heating a Mo boat under a constant flow of argon for 60 minutes in a vacuum chamber.

In last decade MoO_2 nanowires have mainly been synthesized by reducing MoO_3 nanowires, but the structural transformation from MoO_3 to MoO_2 has been seldom studied. In 2009, Hu *et al.*[34] prepared MoO_3 nanowires using a $MoO_3{\cdot}nH_2O$ solution through the hydrothermal technique, and obtained MoO_2 nanowires via hydrogen reduction of the as-synthesized MoO_3 nanowires. They then

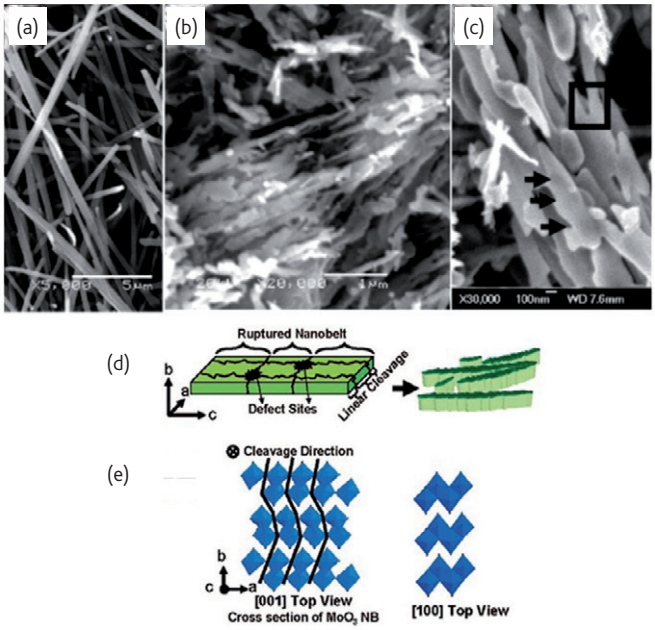

Fig. 3 (a) SEM image of MoO_3 nanowire templates. (b) Low and (c) high magnification images of MoO_2 nanowires. (d) Schematic illustration of the transformation from MoO_3 nanowires to MoO_2 nanowires and (e) a different top view of a MoO_3 layered structure with the cleavage direction. Reprinted with permission from[34]. © 2009 American Chemical Society.

investigated the growth mechanism of one-dimensional MoO_2, which can be explained by the cleavage process, due to defects in the MoO_3. The decrease of length and width was attributed to the cleavage mechanism and the presence of defects in the MoO_3 nanowire. The morphology and transformation mechanism are shown in Fig. 3.

Several molybdenum oxides also have important properties, and thus it has been necessary to explore approaches for preparing nanowires from multiple molybdenum oxides. The liquid phase method is a traditional approach for preparing multiple molybdenum oxide nanowires, and it is hoped that other kinds of flexible method will be available in the future. Dong *et al.*[35] synthesized large scale and homogeneous bunched lead molybdate nanowires via a vertically supported liquid membrane system in the presence of ethylenediamine. Ghorai *et al.*[36] prepared bismuth molybdate (α-$Bi_2Mo_3O_{12}$ phase) nanowires through a pyridine intercalative sonochemical route. Thongtem *et al.*[37] reported reactions using microwave radiation to synthesize multiple molybdenum oxide nanowires.

By reviewing the synthesis of MoO_x nanowires, it has been shown that molybdenum oxide nanowires can be synthesized using many different techniques, such as the gas and liquid phase methods. Template technology can be adopted for controlling the morphology and orderliness of the MoO_x nanowires. Self-assembled nanowires are of great importance in the design and fabrication of nanowire based devices. However, optimizing nanowire positioning, growth direction, morphology, and crystal structure (hexagonal/cubic) requires greater knowledge of the conditions under which one-dimensional crystals preferentially form, and how the various growth mechanisms differ from each other.

Device assembly and properties

Once a nanowire has been grown it must be connected to the outside world. Thanks to the unique properties of MoO_x nanowires, basic device functions are readily achievable with this material, such as energy storage, photocalalysis, field-emission displays, electronic transport, and photodetection.

Battery device assembly and Li storage performance

Li and Li-ion batteries for portable electronic devices and hybrid electric vehicles are becoming increasingly important in today's society[38-42]. Nanostructured MoO_3 has been extensively investigated as a key material for fundamental research and technological applications in electrochemical storage. The reversible electrochemical behavior of the crystalline MoO_3 can be explained by the following redox reaction, which is known to be topotactic[43]:

$$xLi^+ + xe^- + MoO_3 = Li_xMoO_3 \quad (1)$$

Orthorhombic molybdenum trioxide is attractive due to its layered crystal structure. The asymmetrical MoO_6 octahedral are interconnected through corner linking along the [100] direction and edge sharing along the [001] direction to form double-layer sheets parallel to the (010) plane. The interesting host lattice is particularly suitable for the Li^+ insertion reaction and its application in secondary lithium batteries has been investigated extensively.

To investigate the Li storage properties of molybdenum oxide nanowires, Li-ion batteries have been assembled. Fig. 4a shows the assembly process of coin cells, which are assembled in an argon filled glove box, with Li metal as a counter electrode and 1 M $LiPF_6$/ethylene carbonate-diethyl carbonate (w/w = 1:1) as the electrolyte.

Mai *et al.*[29] found that the first discharge capacity of MoO_3 nanowires is 301 $mAh{\cdot}g^{-1}$, which is higher than that for bulk MoO_3 measured under the same conditions. Hexagonal molybdenum trioxide (h-MoO_3) is a metastable phase of molybdenum oxides. However, the basic structural unit is still a distorted octahedron of MoO_6 of ReO_3-type, consisting of a three-dimensional array of corner-sharing MoO_6 octahedra. This open structure not only permits the ready intercalation of some monovalent cations including Na^+, K^+, and NH^{4+}, but also allows them to be readily mobile in the tunnels. Song *et al.*[7] reported that h-MoO_3 exhibited excellent electrochemical performance: the first reversible discharge specific capacity can reach 402 $mAh{\cdot}g^{-1}$, versus Li metal at 0.1 $mA{\cdot}cm^{-2}$ (voltage range 1.2 – 4.0 V).

Layered MoO_x has the potential to offer much higher capacities compared to other metallic oxides. Unfortunately, these materials suffer from poor kinetics and/or a serious capacity fade with cycling,

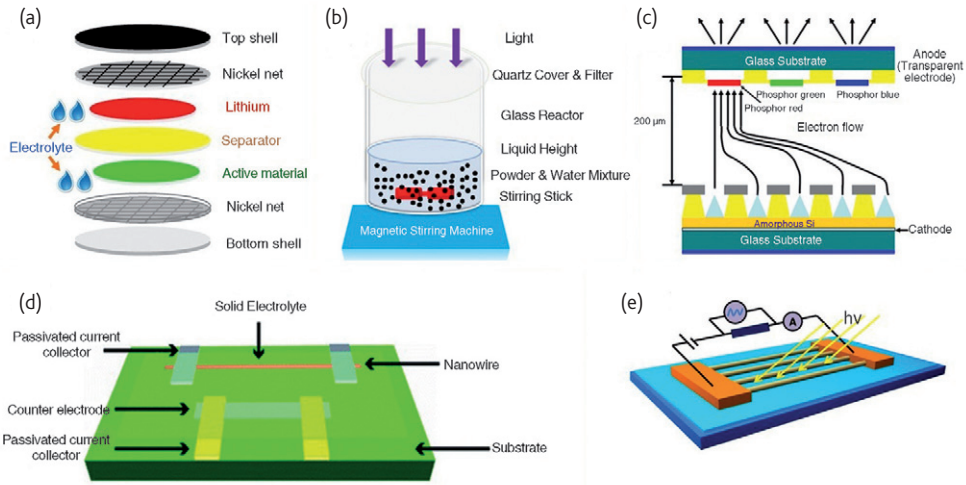

Fig. 4 Schematic of (a) the assembly of the fastening cell, (b) the photocatalytic testing reactor, (c) the structure of a Spindt-type FED, (d) the assembly of single nanowire device, and (e) the optical detection device.

especially at higher rates. Extensive investigations are presently being devoted to overcome these problems through doping[44], as well as by using conductive polymers[45] and carbon coatings[46]. However, adding conductive polymers will make the battery less stable at higher temperatures and carbon coatings will lower the volumetric energy density. Lithiation is considered an effective way of increasing the cycling stability of the cathode and/or anode materials as well as investigating structural changes of the electrode materials during lithium ion insertion. Compared with pristine materials, the lithiated samples exhibit a better cycling capability[11].

Mai *et al.*[29] reported the electroactivity of α-MoO_3 nanowires after lithiation, which demonstrated superior performance to the non-lithiated α-MoO_3 nanowires. Fig. 5 shows the curves of discharge capacity versus the cycle number for the non-lithiated and lithiated MoO_3 nanowire at a current density of 30 mA·g^{-1} and at a temperature of 25 °C. For the non-lithiated MoO_3 nanowire, the discharge capacity decreased to 180 mAh·g^{-1} after 15 cycles, corresponding to a capacity retention of 60 %. However, the discharge capacity of the lithiated MoO_3 nanowire decreased to 220 mAh·g^{-1} after 15 cycles, corresponding to a capacity retention of 92 %, showing the stability and enhanced performance of the lithiated nanowire.

There are only a handful of studies in the literature on MoO_2 despite reports that MoO_2 may be useful as an anode material in Li-ion batteries, as it has demonstrated[47] a relatively large capacity of about 400 – 600 mAh·g^{-1}. Shi *et al.* found that mesoporous MoO_2 material exhibits a reversible electrochemical lithium storage capacity as high as 750 mAh·g^{-1} at C/20 after 30 cycles, making it a promising anode material for lithium ion batteries[6].

The lithium storage capabilities of multiple molybdenum oxides have received the least attention by far[13-15]. Most research has focused on their possible application as anode materials, but their possible use as cathode materials still remains largely unexplored. Xiao *et al.*

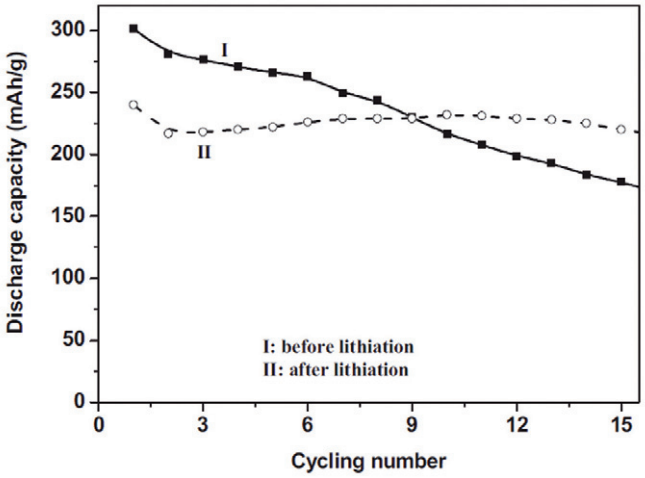

Fig. 5 Curves of discharge capacity versus the cycle number for the non-lithiated and lithiated MoO_3 nanowire. Reprinted from[29]. Copyright Wiley-VCH Verlag GmbH & Co. KGaA. Reproduced with permission.

reported the lithium storage capability of $AMoO_4$ (A = Ni, Co) nanowires: when cycled in the voltage window of 1.5 – 3.5 V, $NiMoO_4$ nanowires manifest a reversible capacity of 100 mAh·g^{-1} after 70 cycles[15].

Photocatalysis

The applications of solar energy conversion and degradation of pollution using semiconductor photocatalysts have received a great deal of attention. To utilize solar energy more effectively, the development of efficient, visible-light-active photocatalysts has attracted worldwide interest[48]. Generally speaking, a photocatalytic reactor consists of two parts: a glass reactor and a lamp. The lamp is positioned above the reactor shown in Fig. 4d. The reaction suspension is prepared by adding nanowires into the simulated wastewater. The

Table 1 Different decolorization rates of bulk MoO_3 and MoO_3 nanowires

Dyes	Methyl violet	Malachite green	Safranine	Rhodamine B
Bulk MoO_3	89.4	86.7	92.6	90.5
MoO_3 Nanowires	99.4	95.3	95.4	97.3

suspension is stirred in the dark to ensure an adsorption/desorption equilibrium before being exposed to UV radiation. The suspension is then irradiated using UV light while being stirred continuously. Analytical samples are removed from the reaction suspension after various reaction times and then the particles are removed using a centrifuge. The supernatant liquor is analyzed by a UV/VIS spectrophotometer.

The photocatalytic properties of MoO_3 nanowires have been studied and the results indicate that MoO_3 nanomaterials demonstrate good photocatalytic ability. Qi *et al.*[49] examined the photocatalytic properties of MoO_3 nanowires by degradation of methyl violet, malachite green, safranine, and Rhodamine B dye solutions. The photocatalytic ability was measured by $D = (A_0 - A) / A_0 \times 100$ %, where A_0 and A are the absorbance of the dye solution before and after illumination, respectively. The results are shown in Table 1, which clearly demonstrate that MoO_3 nanowires exhibit superior photocatalytic abilities over bulk MoO_3. This may be attributed to the large surface area and an extremely high absorption capacity of the nanowires. Moreover, as the energy gap of MoO_3 nanowires turns out to be wider than that of the bulk materials, electrons excited by photons have a more negative potential, which heightens their reducibility. So too, for the oxidability of excited holes, which may be another reason for the enhanced photocatalytic properties of MoO_3 nanowires.

Field emission devices

In 1928 Fowler *et al.* established metallic field emission theory. Investigations associated with field emission theory and field emission devices (FEDs) aroused great interest. The structural diagram of an FED is shown in Fig. 4c. Under the excitation of high-energy electrons the nanowires will emit electrons that can be collected to form a cathode luminescence (CL) image. The Fowler-Nordheim (F-N) formula can be applied to describe the characteristics of field emission materials.

$$J = \frac{A\beta^2 E^2}{\Phi}\exp\left(-\frac{B\Phi^{3/2}}{\beta E}\right) \quad (2)$$

Here, J is the current density, E is the local electric field near the emitter tip, and Φ is the work function of the nanowire. β is the field enhancement factor, which is related to the real electrical field at the tip.

Zhou *et al.*[33] found that MoO_x nanowires exhibited excellent field emission properties. The field emission measurement was carried out in a vacuum chamber of ~2.0×10^{-7} Torr at room temperature.

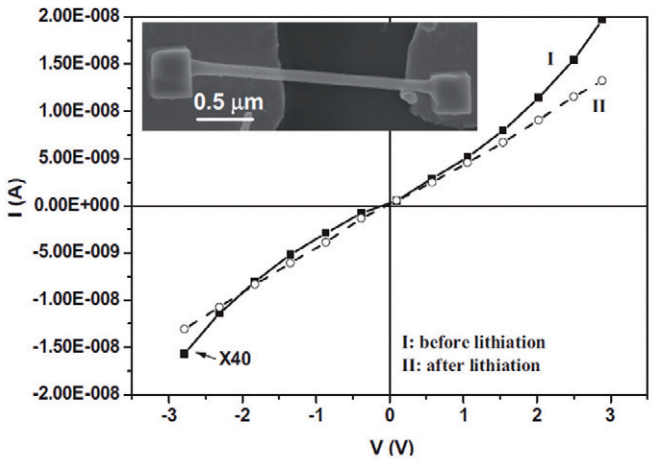

Fig. 6 I-V transport measurements of single nanowire fabricated devices, using samples before and after lithiation. Reprinted from[29]. © Wiley-VCH Verlag GmbH & Co. KGaA. Reproduced with permission.

The turn-on field (E_{to}) and threshold field (E_{thr}) are defined to be the macroscopic fields required to produce a current density of 10 μA·cm^{-2} and 10 mA·cm^{-2} respectively. E_{thr} of the MoO_2 and MoO_3 nanowire arrays was 5.6 MV·m^{-1} and 7.65 MV·m^{-1}, respectively. These values are higher than the best data from carbon nanotubes and SiC nanowires.

In 2006, an investigation on the field emission performance of the MoO_2 nanowires was carried out in a chamber with a vacuum level of ~2×10^{-7} Pa at room temperature[50]. Liu *et al.* found that the alignment of the nanorods played a significant role in the field emission properties. The increase in field emission of the nanorods can be attributed to their sharpened tips. For a given material, it has been demonstrated that a material with high aspect ratio, sharp tips, and abundant edges can greatly increase FE performance. Therefore, investigations on the effects of the factors influencing the field emission properties and successful control of these factors are essential for the application of these nanostructures in real devices.

Single nanowire devices and electrical transport

Nowadays, investigations on the electrical properties of one-dimensional nanomaterials are focused on bulk-forms for order/disorder nanotubes and nanowires[51-56]. As the critical scale of an individual device becomes smaller and smaller, the electron transport properties of their components become an important aspect to study[57]. Mai *et al.*[58] studied the intrinsic reasons for electrode capacity fading in Li-ion based energy storage devices using *in situ* probing of single nanowire electrode devices in 2010. In these devices, a single nanowire was used as a working electrode, and the electrical transport of the single nanowire was recorded *in situ* to detect the evolution of the nanowire during charging and discharging. The work demonstrates the direct relationship between electrical transport, structure, and electrochemical properties of a single nanowire electrode, which will be a promising and straightforward way for nanoscale battery diagnosis.

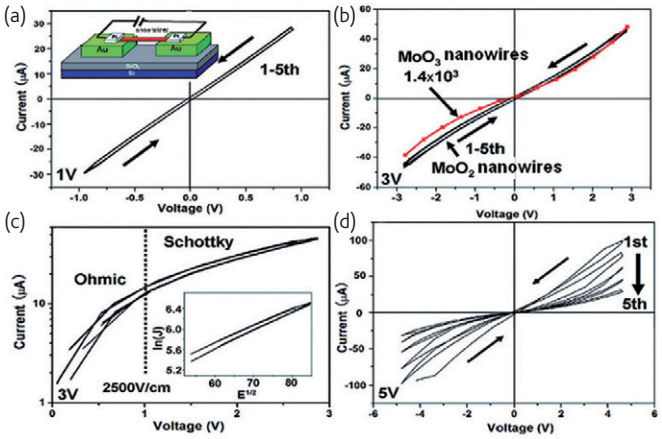

Fig. 7 (a) I-V characteristics of an individual MoO_2 nanowire at 1 V. Inset: schematic view of an individual nanowire device. (b) I-V curves of MoO_2 and MoO_3 nanowires at 3 V. (c) Positive part of the I-V characteristics of the MoO_2 transversal system in (b), shown as a function of log(I). Inset: experimental plot of ln(J) versus $E^{1/2}$ with the electric field above 2500 V/cm. (d) The conductivity of the MoO_2 nanowire changed with the increase of the sweeping time at 5 V. Reprinted with permission from[34]. © 2009 American Chemical Society.

In 2007, Mai *et al.*[29] assembled a single nanowire device to measure the electrical transport through a single MoO_3 nanowire before and after lithiation, to understand the superior performance of lithiated nanowires for Li^+ storage. A single nanowire was placed across two gold electrodes, and the final contacts were improved by Pt deposition at the two ends. Before lithiation, the I-V characteristics of the nanowire showed asymmetric Schottky barriers at the two ends (the solid curve in Fig. 6), as created between the semiconductor MoO_3 (with a band gap of 3.1 eV) and Au/Pt electrodes; the transported current was on the order of ca. 300 pA at ca. 2 V. After lithiation, the I–V curve demonstrated Ohmic behavior (the dashed curve in Fig. 6), and the transported current was of the order of 10 nA at a bias of ca. 2 V. This result suggests that the Li^+ ions introduced during lithiation effectively converted the MoO_3 nanowire behavior from semiconductor to metallic. Using the measured resistance, the effective length, and cross-section of the nanowire, the conductivity was evaluated to be approximately 10^{-4}S·cm^{-1} and 10^{-2}S·cm^{-1} before and after lithiation, respectively. Because the nanowire grows along [001], the increase of conductivity along the nanowire implies an increase of carrier density in the MoO_6 octahedral layers. This suggests that Li^+ ions have been introduced as interstitials into the layers. The work provides a possible explanation as to why the performance of lithiated nanowires is superior to that of non-lithiated ones.

To understand the performance of MoO_2 nanowire, Hu *et al.*[34] measured the electrical transport through an individual MoO_2 nanowire for the first time. The inset in Fig. 7a shows a schematic view of the device. The I-V characteristics were measured by sweeping the bias voltage from negative to positive for five cycles, as shown in Figs. 7a,b,d. The observed behavior is symmetrical and behaves linearly dependent for I vs V in the low voltage range (Fig. 7a), which is in agreement with Ohm's law, and the voltage scan for five cycles does not change the I-V curve. The Ohmic behavior at electric fields below 2500 V·cm^{-1} is due to the existence of delocalized electrons in the conduction band, and the conductivity of an individual MoO_2 nanowire is estimated to be 190 S·cm^{-1} at room temperature. Schottky emission is responsible for the behavior above 2500 V·cm^{-1}. The investigation of the electrical transport along a single MoO_2 nanowire lays the foundation for further investigations toward exploiting MoO_2 nanodevices.

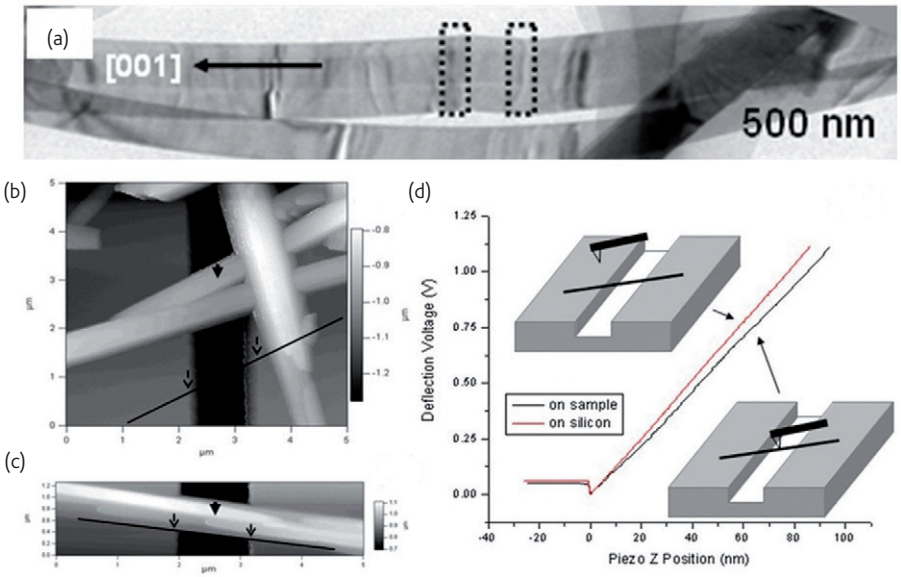

Fig. 8 (a) High magnification TEM image of MoO_3 nanowires, indicating the crumpled characteristics of the MoO_3 nanowires. (b,c) Two typical AFM images of the MoO_3 nanowire samples. The big solid arrowheads indicate the locations of where the forces were applied. The distance between two small dashed arrowheads shows the equivalent length of the nanowires over the trenches. (d) Two typical force-distance curves on the center point of a nanowire and on the silicon substrate, respectively.

Mechanical properties of single nanowires

To integrate the nanowire into functional nanodevices, the mechanical properties must be accurately known, as failure of these building blocks may lead to the malfunction or failure of entire devices[59-61]. Recently our group investigated the intrinsic mechanical performance of individual MoO_3 nanowires, and an interesting relationship between the crumpled nanowires and their elastic properties was found. To perform three-point bending tests on MoO_3 nanowires, well-defined trench patterns were fabricated on a silicon substrate, and both ends of the nanowires were held by two other nanowires (Fig. 8a,b).

Fig. 8c shows two typical force-distance curves on the center point of the suspended nanowire and on the Si substrate. The clamped-clamped beam model (CCBM) is used to simulate the whole mechanical response of the nanowire[62]. According to the CCBM formula:

$$E = \frac{FL^3}{48Iv} = \frac{K_{\mathrm{eff}}L^3}{48I} \tag{3}$$

Where E is the bending modulus, F the force applied, I the moment of inertial given by $wh^3/12$ for the rectangular beam, v the deflection of the suspended nanowire. Also,

$$K_{\mathrm{eff}} = \frac{K_{\mathrm{lever}}S_{\mathrm{Si}}}{S_{\mathrm{sample}} - S_{\mathrm{Si}}} \tag{4}$$

where K_{lever} is the spring constant of the cantilever, S is the sensitivity, which is the inverse of the slope of the F-d curve[63], the bending modulus E can be calculated. For the MoO_3 nanowire, the average value of the elastic modulus is 31 GPa. Compared with bulk MoO_3, with an elastic modulus value of 540 GPa, the elastic modulus has decreased approximately by 94 %. The decrease in elastic modulus is probably attributed to the high surface-to-volume ratio of the MoO_3 wire[64]. Unlike atoms locked in the lattice, surface atoms are less constrained, thereby making the MoO_3 nanowire easier to deform in the elastic regime, and consequently leading to a lower elastic modulus. The low elastic modulus and the nature of layered structure of MoO_3 nanowires is a reasonable explanation for the formation of the crumpled morphology observed in Fig. 8a. These results provide some direct evidence for the mechanism responsible for the plastic deformation of a nanowire when it undergoes mechanical stretching or compression. This approach can be further extended to examine the atomic events occurring during the plastic failure of various metals and their alloys[57].

Photodetection

Photodetectors are devices that detect light by converting optical signals into electrical current. The schematic of a photodetector device is shown in Fig. 4e. Si/SiO_2 substrates with predeposited Ti/Pt gap-cell electrodes are used for electrical characterization. A nanowire is deposited and then connected to the predeposited electrodes. Lead wires of Au were joined to the Pt/Ti electrode pads with Ag paste. No photocurrent was detected between the blank electrodes (i.e., without a nanowire) or between the electrodes and the Si layer. The white light of a light-emitting diode and a Xe lamp were used as light sources to observe the photoconductance as a function of turning the light on and off.

So far, most of the reported nanowire photodetectors are terminal devices. In general, for this type of photodetector there exists a trade-off between the performance parameters, such as current responsivity (R_λ), photoresponse ratio ($I_{\mathrm{light}}/I_{\mathrm{dark}}$), and the photoresponse time (rise and decay times). For practical use, exploring new ways to develop single photodetectors with an overall enhancement in the performance is critical[65,66].

Makise *et al.*[67] have fabricated MoO_x nanowires that are grown on a SiO_2 substrate by electron-beam-induced deposition (EBID) using a $Mo(CO)_6$ precursor with O_2. They found that the nanowire can be reversibly switched between low and high conductivity. As the Xe lamp (the wavelength is 400 nm) was switched on, the conductance jumped from 2.2×10^{-4} to 3.6×10^{-4} S in 5.9 s. The characteristics of the MoO_x nanowires suggest that they are promising candidates for photodetectors and optical switches. Optimization of nanowire composition may improve the optical sensitivity and photo-response.

Conclusions and outlook

This article provides an overview of a variety of chemical methods that have been developed for generating MoO_x nanowires. We have also discussed a range of interesting properties associated with MoO_x nanowires. Preliminary results from many research groups have explored how MoO_x nanowires may be used as a functional building block for electronics, photonics, and mechanical sensors. MoO_x nanowire devices have been fabricated, and the novel physical/chemical properties investigated[68-70].

MoO_x nanowires and their nanowire device applications are still in the early stage of technical development. To be of real interest to industry, a number of issues must be addressed. First of all, generic issues related to epitaxy still need to be systematically studied. For example, improving the crystal quality of the desired MoO_x nanowire with high power and high rate performance represents a significant step toward practical application in lithium-ion batteries. Also, searching for new molybdenum oxides with special coordination

Instrument citation

D/MAX-TTRIII, x-ray diffractometer, Rigaku
JSM-5610LV, scanning electron microscope, JEOL
JEM-2010 FEF, transmission electron microscope, JEOL
BTS-5V/5 mA, battery Testing System, Neware
Molecular force probe MFP-3, mechanical testing system, Asylum Research
SR570, electrical testing system, Stanford Research Systems
NOVA 200, focused ion beam microscope, FEI

characteristics is also expected to significantly enhance its use in energy-saving devices. The second challenge faced by chemically synthesized nanowires regards the modification. MoO_x is a kind of semiconductor; it can be doped to conduct with negative electrons or positive holes, enabling p-n junctions and transistors to be formed. The possibility of controlling the conductivity and carrier type of MoO_x by adding impurities is the subject of forthcoming investigations. The third challenge is the self assembly of MoO_x into complex structures or device architectures. For example, hierarchical structured nanowire networks, which can be based on functional MoO_x nanowires, are necessary for creating devices. Recent advances in nanoscience and nanotechnology open up a myriad of opportunities for a new generation of devices based on MoO_x nanowires. Looking forward, the future appears remarkably bright, and the application of MoO_x nanowire devices is expected to greatly expand the impact of these materials on science and industry. mt

Acknowledgement

This work was partially supported by the National Nature Science Foundation of China (50702039, 51072153), program for New Century Excellent Talents in University (NCET-10-0661), the Research Fund for the Doctoral Program of Higher Education (20070497012), the Fundamental Research Funds for the Central Universities (2010-II-016), and Scientific Research Foundation for Returned Scholars, Ministry of Education of China (2008-890). We express our deep thanks to Professor C. M. Lieber of Harvard University, Professor Z. L. Wang of Georgia Institute of Technology, Professor W. J. Mai of Jinan University and Dr. Y. J. Dong, Professor Y. Shao of Massachusetts Institute of Technology for fruitful collaboration and stimulating discussion.

REFERENCES

1. Brezesinski, T., *et al.*, *Nat Mater* (2010) **9**(2), 146.
2. Tian, B., *et al.*, *Science* (2010) **329**(5993), 830.
3. Tian, B., *et al.*, *Nature* (2007) **449**(7164), 885.
4. Wang, Z. L., and Song, J., *Science* (2006) **312**(5771), 242.
5. Ramana, C. V., *et al.*, *Solid State Commun* (2009) **149**(1-2), 6.
6. Shi, Y., *et al.*, *Nano Lett* (2009) **9**(12), 4215.
7. Song, J., *et al.*, *Mater Res Bull* (2005) **40**(10), 1751.
8. Marin Flores, O. G., and Ha, S., *Appl Catal A* (2009) **352**(1-2), 124.
9. Marin-Flores, O., *et al.*, *J Nanoelectron Opt* (2010) **5**, 110.
10. Tangestaninejad, S., *et al.*, *Inorg Chem Commun* (2008) **11** (3), 270.
11. Mai, L. Q., *et al.*, *J Mater Res* (2010) **25**(8), 1413.
12. Mai, L. Q., *et al.*, *Int J Electrochem Science* (2008) **3**(2), 216.
13. Ding, Y., *et al.*, *Inorg Chem* (2008) **47**(17), 7813.
14. Sharma, N., *et al.*, *Chem Mater* (2003) **16**(3), 504.
15. Leyzerovich, N. N., *et al.*, *J Power Sources* (2004) **127**(1-2), 76.
16. Xiao, W., *et al.*, *Chem Mater* (2009) **22**(3), 746.
17. Smith, P. A., *et al.*, *Appl Phys Lett* (2000) **77**(9), 1399.
18. Scanlon, D. O., *et al.*, *J Phys Chem C* (2010) **114**(10), 4636.
19. Cui, Y., and Lieber, C. M., *Science* (2001) **291**(5505), 851.
20. Lieber, C. M., and Wang, Z. L., *MRS Bull.* (2007) **32**, 99.
21. Tenne, R., *et al.*, *Nature* (1992) **360**(6403), 444.
22. Margulis, L., *et al.*, *Nature* (1993) **365**(6442), 113.
23. Almana, D. E., *et al.*, *Mater Sci Eng* (1992) **155**(1-2), 85.
24. Huang, J. M., and Kelley, D. F., *Chem Mater* (2000) **12**(10), 2825.
25. Zach, M. P., *et al.*, *Science* (2000) **290**(5499), 2120.
26. Satishkumar, B. C., *et al.*, *J Mater Chem* (2000) **10**(9), 2115.
27. Niederberger, M., *et al.*, *J Mater Chem* (2001) **11**(7), 1941.
28. Wang, S., *et al.*, *Solid State Commun* (2005) **136**(5), 283.
29. Mai, L. Q., *et al.*, *Adv Mater* (2007) **19**(21), 3712.
30. Chen, W., *et al.*, *J Phys Chem Solids* (2006) **67**(5-6), 896.
31. Cai, L., *et al.*, *Nano Lett* (2011) **11**(2), 872.
32. Zhang, S. L., and d'Heurle, F. M., *Appl Phys Lett* (2000) **76**(14), 1831.
33. Zhou, J., *et al.*, *Adv Mater* (2003) **15**(21), 1835.
34. Hu, B., *et al.*, *ACS Nano* (2009) **3**(2), 478.
35. Dong, F.Q., and Wu, Q.S., *Appl Phys A* (2008) **91**(1), 161.
36. Ghorai, T. K., *et al.*, *J Alloys Compd* (2008) **463**(1-2), 390.
37. Thongtem, T., *et al.*, *Curr ApplPhys* (2008) **8**(2), 189.
38. Mai, L. Q., *et al.*, *Nano Lett* (2010) **10**(11), 4750.
39. Goodenough, J. B., *J Power Sources* (2007) **174**(2), 996.
40. Ma, M., *et al.*, *J Power Sources* (2007) **165**(2), 517.
41. Ji, X., *et al.*, *Nat Mater* (2009) **8**(6), 500.
42. Miller, J. R., *et al.*, *Science* (2010) **329**(5999), 1637.
43. Yu, A., *et al.*, *Solid State Ionics* (1998) **106**(1-2), 11.
44. Lee, Y., *et al.*, *Nano Lett* (2008) **8**(3), 957.
45. Huang, X. H., *et al.*, *Electrochem Commun* (2008) **10**(9), 1288.
46. Doherty, C. M., *et al.*, *Chem Mater* (2009) **21**(21), 5300.
47. Yang, L. C., *et al.*, *Electrochem Commun* (2008) **10**(1), 118.
48. Shang, M., *et al.*, *J Phys Chem C* (2009) **113**(33), 14727.
49. Qi, Y. Y., *et al.*, *J Wuhan Univ Technol* (2007) **29**(7), 1671.
50. Liu, J., *et al.*, *Mater Lett* (2004) **58**(29), 3812.
51. Duan, X., *et al.*, *Nature* (2001) **409**(6816), 66.
52. Wang, J., *et al.*, *Science* (2001) **293**(5534), 1455.
53. Huang, Y., *et al.*, *Science* (2001) **291**(5504), 630.
54. Wang, W. Z., *et al.*, *Adv Mater* (2006) **18**(24), 3275.
55. Wan, Q., *et al.*, *Appl Phys Lett* (2007) **90**(22), 222107.
56. Heo, Y. W., *et al.*, *Appl Phys Lett* (2004) **85**(11), 3.
57. Xia, Y., *et al.*, *Adv Mater* (2003) **15**(5), 353.
58. Mai, L., *et al.*, *Nano Lett* (2010) **10**(10), 4273.
59. Wu, B., *et al.*, *Nat Mater* (2005) **4**(7), 525.
60. Tabib-Azar, M., *et al.*, *Appl Phys Lett* (2005) **87**(11), 113102.
61. Wen, B., *et al.*, *Phys Rev Lett* (2008) **101**(17), 175502.
62. Kopidakis, N., *et al.*, *Appl Phys Lett* (2006) **89**(10), 103524.
63. Gao, P. X., *et al.*, *Science* (2005) **309**(5741), 1700.
64. Amos, F. F., *et al.*, *J Am Chem Soc* (2007) **129**(46), 14296.
65. Ye, Y., *et al.*, *ACS Appl Mater & Interfaces* (2010) **2**(12), 3406.
66. Yang, Q., *et al.*, *ACS Nano* (2010) **4**(10), 6285.
67. Makise, K., *et al.*, *Nanotechnology* (2009) **20**(42), 425305.
68. Mariotti, D., *et al.*, *Nanotechnology* (2008) **19**(49), 495302.
69. Rajeswari, J., *et al.*, *Electrochem Commun* (2009) **11**(3), 572.
70. Gao, Q., *et al.*, *J Mater Chem* (2010) **20**(14), 2807.